Self-Assembly of Graphene Nanostructures on Nanotubes

Niladri Patra, Yuanbo Song, and Petr Král*

Department of Chemistry, University of Illinois at Chicago, Chicago, Illinois 60607, United States

ABSTRACT We demonstrate by molecular dynamics simulations that carbon nanotubes can activate and guide on their surfaces and in their interiors the self-assembly of planar graphene nanostructures of various sizes and shapes. Nanotubes can induce bending, folding, sliding, and rolling of the nanostructures in vacuum and in the presence of solvent, leading to stable graphene rings, helices, and knots. We investigate the self-assembly conditions and analyze the stability of the formed nanosystems, with numerous possible applications.

KEYWORDS: molecular dynamics · self-assembly · graphene · carbon nanotube · nanostructures

Recently, graphene monolayers have been prepared and intensively studied.[1−4] Graphene nanoribbons (GNRs) have also been synthesized[5−8] and prepared from graphene monolayers and carbon nanotubes (CNTs) by lithographic[9,10] and catalytic methods.[11,12] Graphene flakes with strong interlayer van der Waals (vdW) coupling and chemical functionalization at their edges can self-assemble into larger structures.[13−15] Highly elastic graphene[16−18] could fold under suitable conditions into nanoscrolls[19−22] and a variety of other 3D nanostructures.[23]

Novel composite functional materials could be prepared if planar graphene nanostructures of various shapes and sizes are self-assembled on the surfaces of nanoscale materials. Highly rigid CNTs, with selective and strong vdW coupling to planar graphene surfaces[24,25] and to molecules adsorbed on them,[26] might form suitable substrates for this graphene self-assembly. Here, we test by atomistic molecular dynamics (MD) simulations if planar graphene nanostructures could self-assemble on CNT surfaces and in their interiors.

RESULTS AND DISCUSSION

GNR Folding Outside and Inside CNTs. In Figure 1, we show how a GNR of the length of $l_G = 40$ nm and the width of $w = 3$ nm rolls on a (60,0) CNT of the length of $l_C = 20$ nm, with its two ends fixed. Initially, the GNR tip is positioned perpendicularly ($\varphi = 0$) to the CNT axis close to its surface. (a) The tip immediately starts to fold on the CNT, due to large vdW coupling. (b) After $t \approx 0.5$ ns, the GNR forms a single layer around the CNT. (c,d) Within another $t \approx 1$ ns, it forms a multilayered ring structure.

We investigate further how the initial angle φ of the GNR with respect to the CNT axis affects the self-assembly processes. In Figure 2a−c, the tip of the GNR (40×2 nm^2) is initially positioned on the same CNT at the angle of $\varphi = 60°$. (a) The tip again folds fast around the CNT. (b,c) After $t = 0.5-1$ ns, it starts to fold around the CNT in a spiral manner. The spiral becomes denser, where the neighboring edges each other, and the GNR eventually forms a stable helical structure. The self-assembly speed is determined by the strength of vdW forces acting on the GNR and the rate of its momentum dissipation, due to friction with the CNT.

We test if GNRs can also fold inside CNTs. As shown in Figure 2d,e, we put a GNR (40×2 nm^2) inside the above CNT. Initially, the ribbon is placed at the CNT entrance, and its orientation is parallel with the CNT axis. (d) First, the GNR sticks to the interior surface of the CNT and starts to enter the CNT in a straight motion. Within $t \approx 0.5$ ns, it reaches the other CNT end, overstretches it, and comes back. The GNR motion eventually loses its straight symmetry and gains a helical form, with a randomly oriented rotation direction. (e) Within several nanoseconds, the helical pitch becomes denser, until it is so dense that the GNR edges touch each other. The helical structure equilibrates and stays in a folded form inside the CNT. We always observe formation of the same helical structure, independently on the initial position of the GNR with respect to the CNT center. However, we can control the helicity of the folded GNR by the initial angle φ.

*Address correspondence to pkral@uic.edu.

Received for review September 24, 2010 and accepted February 9, 2011.

Published online February 22, 2011
10.1021/nn102531h

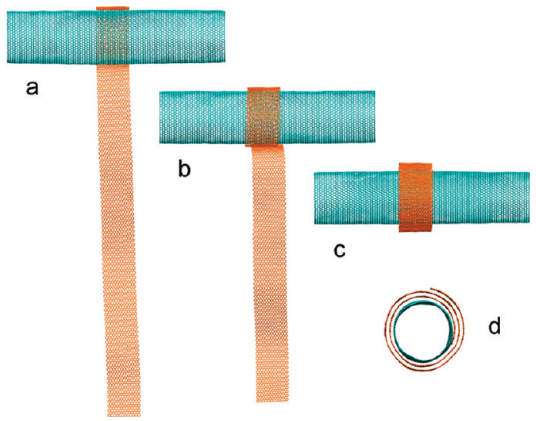

Figure 1. Rolling of a GNR (40 × 3 nm^2) on a (60,0) CNT when placed close to the CNT perpendicular to its axis (movie in Supporting Information).

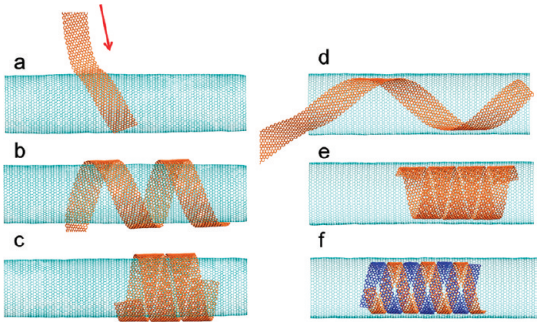

Figure 2. (a−c) Helical rolling of a GNR (40 × 2 nm^2) when placed at the angle of $\varphi = 60°$ with respect to the axis of the l = 20 nm (60,0) CNT. (d,e) Same when this GNR is placed inside this CNT (front part of the CNT is removed for better visualization). (f) Final structure of two GNRs (40 × 1 nm^2) when placed inside this CNT (movies in Supporting Information).

We also study folding of two GNRs (40 × 1 nm^2) inside this CNT. Initially, the GNRs are placed on the top of each other and placed at one CNT entrance. Upon release, both GNRs start to move in parallel inside the CNT. After $t \approx 1$ ns, they start to fold in a helical manner in the same direction. Within $t \approx 3$ ns, the two GNRs form a double helical structure, as shown in Figure 2f. While the helical orientation of the two GNRs can be controlled by the initial angle φ, the two equilibrated GNRs always end up having the same orientations. When we simultaneously place more GNRs on the surface or in the interior of CNT, the GNRs tend to fold side by side rather than on the top of each other. This is caused by smaller GNR deformation energies and larger GNR−CNT vdW attractions (geometrical overlap). However, GNRs can fold on each other if we release the second GNR later.

In Figure 3, we summarize in phase diagrams the structures obtained in MD simulations of GNR folding outside long CNTs ($l_C \gg l_G$). All of these (stable or metastable) structures are obtained by initially placing the GNRs in contact with the CNTs and then releasing them. The structures are presented in dependence on

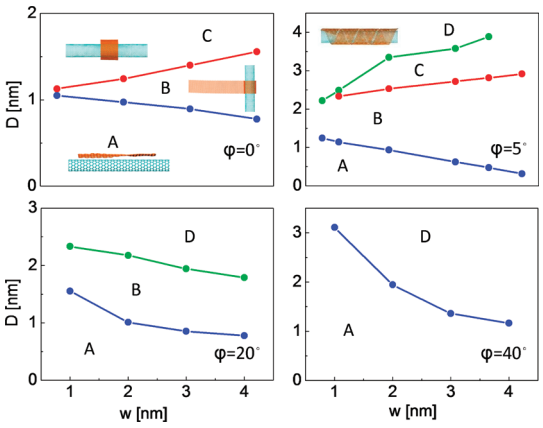

Figure 3. Phase diagrams of GNRs of the width w self-assembled on long CNTs of the diameter D_C, shown for different initial angles φ with respect to the CNT axis. The GNRs self-assemble into nanostructures called the (A) straight, (B) nonfolding, (C) rolling, and (D) helical phases.

the CNT diameter, D_C, the GNR width, w, and the initial angle, φ, of the GNR with respect to the CNT axis. We display four types of structures, called the (A) straight, (B) nonfolding, (C) rolling, and (D) helical phases. For small angles, $\varphi < 5°$, we obtain the A, B, and C phases, as shown in Figure 3 (top left). When we increase the angle to $\varphi \approx 5-15°$, the D phase appears for large CNTs, as shown in Figure 3 (top right). At larger angles, $\varphi > 20-30°$, the C phase disappears, as seen in Figure 3 (bottom left). When the angle is further increased, $\varphi > 30°$, the B phase disappears, as well, as seen in Figure 3 (bottom right). Analogously, we can obtain phase diagrams for the self-assembly of GNRs inside CNTs and in other cases of interests.

Analytical Model. We use a simple analytical model to understand the conditions under which GNRs self-assemble into different structures outside and inside CNTs. We describe the total CNT−GNR coupling energy in the form

$$\begin{aligned} E_{\text{total}} &= E_{\text{ela}} + E_{\text{C-G}} + E_{\text{G-G}} \\ E_{\text{C-G}} &= \sum_{i\text{-CNT},\, j\text{-GNR}} V_{i,j} = \langle E_{\text{C-G}} \rangle + E_{\text{sym}} \\ E_{\text{G-G}} &= \sum_{i,\, j\text{-GNR}} V_{i,j} \end{aligned} \qquad (1)$$

Here, E_{ela}, E_{C-G}, and E_{G-G} are the bending energy of GNRs, the vdW binding energy between CNTs and GNRs, and the vdW energy for coupling of neighboring layers or edges of GNRs, respectively. The i,j indices in the Lennard-Jones potential, $V_{i,j}$, of the form shown in eq 4, run over atoms in the two subsystems.

The bending energy is given by $E_{ela} = \sigma_{ela} A_{ela}$, where σ_{ela} is the strain energy density and A_{ela} is the total bending area.[27,28] In the linear elastic regime, $\sigma_{ela} = D\kappa^2/2$, where $\kappa = (\kappa_1 + \kappa_2)/2$ is the local mean curvature and D is the flexural rigidity. When a GNR folds on a CNT, one of the two curvatures is $\kappa_{1(2)} \approx 0$. Then, the curvature is given by $\kappa = R_G^{-1}$, where R_G is the radius of the folded GNR.

As shown in eq 1, the coupling energy, E_{C-G}, can be split into the "mean-field" term, $\langle E_{C-G}\rangle$, and the "symmetry-related" term, E_{sym}. The first term represents the vdW coupling between CNT and GNR lattices that is averaged over the angle describing mutual orientation of the two subsystems (smearing of their hexagonal lattices). The symmetry-related term accounts for the difference between the actual and smeared coupling (interferences) of the lattices in the CNT and GNR structures.[24,25] Due to the last term, the GNR might have local potential energy minima for certain orientations with respect to the CNT (symmetry locking).

The full CNT−GNR coupling energy can be expressed as $E_{C-G} = -\sigma_{C-G}A_{C-G}$, where σ_{C-G} is the related (positive) energy density and A_{C-G} the related coupling area. Analogously, we can write the averaged and symmetry terms as $\langle E_{C-G}\rangle = -\langle\sigma_{C-G}\rangle A_{C-G}$ and $E_{sym} = -\sigma_{sym}A_{C-G}$, respectively. We estimate the σ_{sym} coefficient by placing a graphene flake with a hexagonal shape on a large graphene sheet.[29] Their binding energies E_{C-G} and E_{sym} have a C_6 symmetry with respect to rotation of the flake around the axis going through its center and orthogonal to the graphene. The GNR−GNR vdW coupling energy (in the case of sidewise coupling) is $E_{G-G} = -\sigma_{G-G}L_{G-G}$, where σ_{G-G} and L_{G-G} are the (positive) sidewise vdW binding energy density and the GNR edge length, respectively. From our MD simulations and $D \approx 27.9$ kcal/mol,[23] we estimate that $\langle\sigma_{C-G}\rangle \approx 56$ kcal/mol/nm^2, $\sigma_{sym} \approx 0.25$ kcal/mol/nm^2, and $\sigma_{G-G} \approx 2.9$ kcal/mol/nm.[29]

Testing of the Analytical Model. We apply eq 1 to several phases observed above. The necessary condition for the realization of the CNT-assisted self-assembly of GNRs is that the total energy in the self-assembled state is smaller than at the beginning (*i.e.*, $E_{total} < 0$ or $E_{C-G} + E_{G-G} < -E_{ela}$). More precisely, the energy should drop in every infinitesimal distortion of the system along the self-assembly trajectory. Therefore, local barriers may prevent the self-assembly in some cases even if $E_{total} < 0$.

First, we find the boundary of the B and C phases shown in Figure 3 (top left); that is, we estimate what is the minimum radius of CNT, $R_C = D_C/2$, on which a GNR can fold for $\varphi = 0$. The folding is driven by the competition between the E_{C-G} and E_{ela} energies. If we neglect the symmetry locking term, E_{sym}, we get $E_{C-G} \approx \langle E_{C-G}\rangle$, and from the folding condition, $E_{tot} = E_{C-G} + E_{ela} < 0$, we obtain

$$\frac{A_{C-G}}{A_{ela}} > \frac{\sigma_{ela}}{\langle\sigma_{C-G}\rangle} \qquad (2)$$

Here, the area where the GNR couples to the CNT is also the bending area of the GNR, $A_{C-G} \approx A_{ela}$. If we assume that $R_C \approx R_G$, we obtain from eq 2 and $\sigma_{ela} = D/2R_C^2$ the condition for the folding of GNR

$$R_C > \sqrt{\frac{D}{2\langle\sigma_{C-G}\rangle}} \qquad (3)$$

For the above values of D and $\langle\sigma_{C-G}\rangle$, eq 3 gives $R_C > 0.5$ nm, in a reasonable agreement with our simulations, giving the minimum value of $R_C \approx 0.7$ nm.

Next, we analyze the A (straight) and D (helical) GNR phases formed inside CNTs. Stabilization of these phases is similar to the cases with external GNR self-assembly, shown in Figure 3. To reproducibly obtain the A phase in the simulations, we need to remove the large initial potential energy of the system; otherwise, the GNR acquires large oscillations which often lead to the helical D phase. We can do so by either placing the GNR (in a straight way) fully inside (outside) the CNT or by using a large Langevin damping constant (>0.1 ps^{-1}).

We evaluate the binding energy in the A phase from eq 1, where we consider a GNR (40×3 nm^2) placed in a straight way inside a (much longer) (60,0) CNT. When the GNR forms a monolayer on the CNT interior, its curvature is roughly the same in all phases. Using the values of $R_G \approx 2$ nm and $A_{ela} = 120$ nm^2, the GNR bending energy is $E_{ela} = \sigma_{ela}A_{ela} = (D/2R_G^2)A_{ela} = 420$ kcal/mol. In the A phase, the GNR and CNT lattices are oriented in the same way, which gives the symmetry locking energy of $E_{sym} \approx -0.25 \times 120 \approx -30$ kcal/mol. Then, considering the fact that $E_{G-G} = 0$, we obtain the total coupling energy of $E_{total} \approx E_{ela} + \langle E_{C-G}\rangle + E_{sym} \approx 420 - 56 \times 120 - 30 \approx -6330$ kcal/mol.

The coupling energy of the (internal) D phase in this CNT can be obtained in the same way. Here, $E_{G-G} \approx -2.9 \times 30 = -87$ kcal/mol, due to partial overlap of the GNR edges, and the symmetry term is $E_{sym} \approx 0$, due to unfavorable angle φ.[29] Therefore, the total coupling energy is $E_{total} \approx E_{ela} + \langle E_{C-G}\rangle + E_{G-G} \approx 420 - 6720 - 87 \approx -6387$ kcal/mol.

From these results, it would seem that the system in the internal A phase is by ≈60 kcal/mol less stable than the D phase. In fact, direct evaluation by VMD[31] of the total energies in these two simulated systems shows that the system in the A phase is by ≈70 kcal/mol more stable than in the D phase. Therefore, the phase A is thermodynamically stable, while the phase D is only kinetically stable. The reason of this inversion might be due to slightly different GNR curvature, CNT deformations, symmetry coupling, and other phenomena not captured in eq 1. For example, if we assume that the radius R_G of the GNR in the A phase is ≈18% larger than that in the D phase, then eq 1 gives the same energy difference between these phases as the simulations.

Next, we test if the previous system can be prepared with a locking angle shifted by 60° from that in the A phase. Since $E_{sym}(2.5\text{ nm}^2) \approx kT = 0.597$ kcal/mol at $T = 300$ K, small GNRs can be easily thermally decoupled from their symmetry-locked positions. Therefore, we simulate the systems at $T = 200$ K and use the Langevin damping coefficient of 0.05 ps^{-1}.

As shown in Figure 4a,b, we can stabilize helical structures with a larger pitch of GNRs locked on the

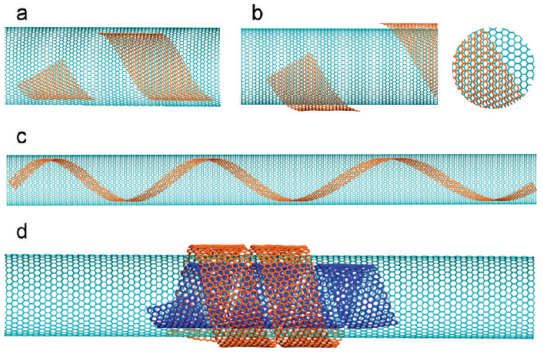

Figure 4. (a) Helical locked GNR (40 × 3 nm^2) inside a (60,0) CNT. (b) Same outside this CNT and detail of the locked structures. (c) Loosely helical folded GNR (60 × 1 nm^2) when it is placed inside the l_C = 50 nm long (60,0) CNT. (d) Two GNRs (25 × 2 nm^2) helical folded and vdW coupled over the wall of the (60,0) CNT (front parts of all the CNTs and GNRs (a,b) are removed for better visualization).

interior (exterior) surface of the (60,0) CNT. The model coupling energy of the locked helical structure in Figure 4a, $E_{total} \approx E_{ela} + \langle E_{C-G} \rangle + E_{sym} \approx 420 - 6720 - 30 \approx -6330$ kcal/mol, is the same as in the A phase. Therefore, the locked helical phase is by ≈60 kcal/mol less stable than the D phase, while VMD gives (at T = 300 K) the energy difference for these systems of ≈80 kcal/mol. When we increase the temperature in the simulations to $T \approx 500$ K, this helical locked structure switches to the D phase.

We continue by examining how GNRs self-assemble inside CNTs of finite lengths when $l_G > l_C$. We place a GNR (60 × 1 nm^2) straight inside a (60,0) CNT (l_C = 50 nm). The GNR tends to maximize its overlap with the shorter CNT, due to vdW binding. Therefore, it forms a loose helical structure with both GNR ends present inside the CNT, as shown in Figure 4c. In contrast to the helical locked cases seen in Figure 4a, b, this structure with a large pitch is stabilized by the finite length of the CNT. Therefore, when the CNT length is shorter, so is the pitch of the helice, until it becomes so dense that the GNR switches to the more stable D phase. The same structures are also formed outside finite CNTs.

We also explore the self-assembly of two GNRs (25 × 2 nm^2) initially placed on the opposite sides of the (60,0) CNT wall. Since the GNRs weakly interact by vdW coupling over the CNT wall, their self-assembly is correlated. As shown in Figure 4d, the GNRs form *overlapping* helical structures on both sides of the wall. It turns out that the external GNR induces the folding of the internal GNR, including its helicity. When the external GNR is removed from the system, the internal GNR does not even fold.

More Complex Nanostructures. In the above-described manner, one could in principle assemble arbitrary planar graphene nanostructures on the surfaces or in the interior of CNTs. Here, we test this idea on the self-

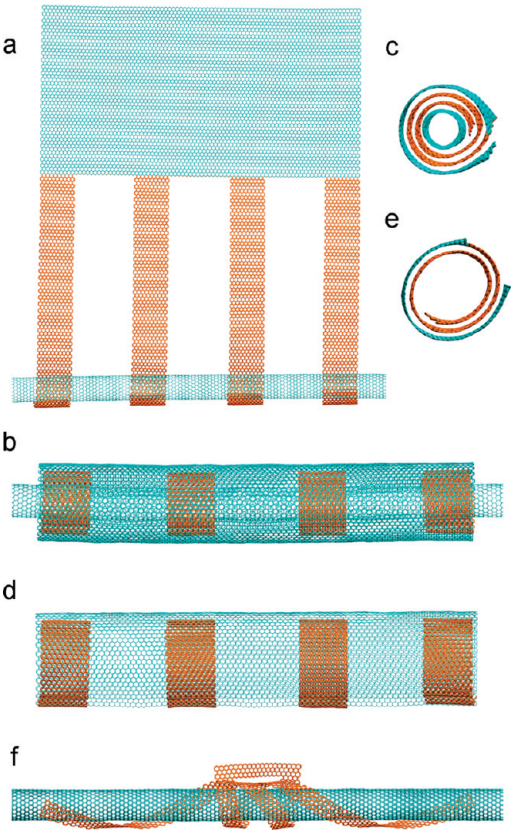

Figure 5. Graphene rings and knot formations from structured graphene flakes self-assembled on the CNT surface. (a−c) Formation of multiple GNR rings, covered with a single layer graphene sheet, on the (20,0) CNT. (d,e) After removal of the CNT, the multiring structure, covered with a single layer graphene sheet, is stabilized. (f) When the (20,0) CNT is placed between two connected GNRs, a complex knot is formed (movie in Supporting Information).

assembly of a "hair-brush"-like graphene nanostructure with four GNRs (60 × 2 nm^2). One end of all four GNRs is connected to the remaining part (40 × 100 nm^2) of the graphene sheet, and the distance between the adjacent GNRs is 5 nm, as shown in Figure 5a. Initially, the tips of all four GNRs are placed on the (20,0) CNT. They start to fold around it, and after $t \approx 4$ ns, they form a single layer ring structures on the CNT. Within another $t \approx 3$ ns, the GNRs make a multilayered ring structure. The rest of the graphene sheet also folds on the multilayered ring structures and eventually completely wraps around the GNRs, as shown in Figure 5b, c. Then, we equilibrate the self-assembled structure, remove the CNT from its core, and equilibrate the remaining folded graphene. Upon removal, the diameter of the four rings slightly expands by 0.2 nm, as shown in Figure 5d,e, but the system retains the same shape, stabilized by the top graphene monolayer.

It is interesting to explore the self-assembly dynamics of such hair-brush structures when the CNT is positioned differently. For simplicity, we use two (20 × 1 nm^2) GNRs, connected to a (5 × 1 nm^2) graphene

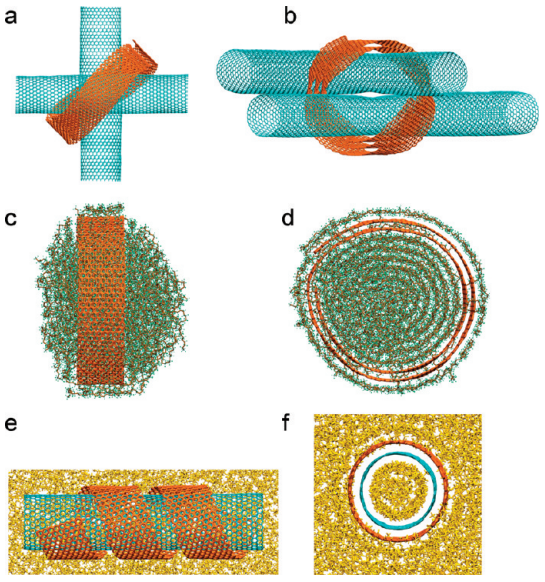

Figure 6. Binding of CNTs and polyethylene by graphene nanoribbons. (a) Top view and (b) side view of two crossed CNTs (20,0), tied by a 60 × 2 nm^2 GNR. (c,d) Polyethylene chains wrapped by a (40 × 2 nm^2) GNR. (e,f) Helical rolling of a GNR (20 × 2 nm^2) when placed at the angle of $\varphi = 60°$ with respect to the axis of the $l = 15$ nm (30,0) CNT in hexane (front part of solvent is removed for better visualization).

sheet, where the distance between the GNRs is 3 nm. Initially, we place a (20,0) CNT with fixed ends perpendicularly between the two GNRs, close to their tips. Within $t \approx 0.5$ ns, the GNRs fold around the CNT. After another $t \approx 1.5$ ns, the GNRs cross each other and make a knot around the CNT. Then the ends of the two GNRs propagate on the CNT surface in a spiral manner and eventually make a tight knot on the CNT, as shown in Figure 5f. This example illustrates that GNR self-assembly can be controlled by positioning the CNTs differently.

GNRs might be also used as nanomechanical connecting materials. We test if such "nanoglue" formed by a GNR (60 × 2 nm^2) can hold together two crossed (20,0) CNTs. Initially, the GNR is folded around two parallel CNTs (one with fixed ends) in a form of multilayered ring structure. After equilibration, we start to rotate one CNT with respect to the other by applying the force of $f = 0.01$ kcal/mol/Å to one of the edge atoms of the CNT with free ends. As the chosen CNT rotates, the GNR ring starts to slightly unfold. Once the CNTs are perpendicular to each other ($t \approx 1.5$ ns), we fix their mutual rotation and obtain the system shown in Figure 6a,b.

Next, we apply the force of $f = 0.01$ kcal/mol/Å, oriented upward, to the edge atoms at both ends of the relaxed CNT. This is the minimum force under which the CNT moves upward. Under this force, the GNR starts to unfold and a 5 nm gap is formed between the two perpendicular CNTs within $t \approx 1$ ns. At this position, we remove the force and allow spontaneous vertical translation of the relaxed CNT. Within $t \approx 1$ ns, the system comes back to its starting position, shown in Figure 6a,b. In order to reproduce the original structure, we should not separate the CNTs by more than ≈5 nm, due to GNR restructuring. We might strengthen the GNR−CNT wrapping by using structured or chemically functionalized GNRs.[32]

We also test if GNRs can wrap around other materials to functionalize, strengthen, or glue them. We take 36 parallel polyethylene [−$(CH_2)_n$−] chains, each with 200 ethylene units. After equilibration for $t = 10$ ns at $T = 300$ K, the polyethylene chains form a bundle. Then we place a (40 × 2 nm^2) GNR tip at the bundle, perpendicularly to its orientations. Initially, the tip starts to form a GNR helix on the bundle. After $t \approx$ 5−10 ns, the helical GNR refolds on the bundle, resembling a roll shown in Figure 1. The GNR also becomes covered with the loose polyethylene chains. As the GNR rolling continues, the polyethylene chains start to roll with the GNR, and within $t \approx 10$ ns, the system acquires the form shown in Figure 6c,d.

Finally, we investigate the self-assembly of GNRs on CNTs solvated in hexane and ethyl alcohol. Initially, a GNR (30 × 3 nm^2) is placed perpendicularly to the surface of solvated (60,0) CNT at $T = 300$ K (NPT ensemble). The GNR tip starts to fold on the CNT, and after $t \approx 1$ ns, it goes once around its circumference. To proceed in hexane (not in ethyl alcohol) further, and form a multilayered ring, as in Figure 1a−d, we need to heat the system to $T = 375$ K. Next, we test folding of the helical structure with the GNR (20 × 2 nm^2) on (30,0) CNT at an angle of $\varphi = 60°$ with respect to the CNT at $T = 300$ K. The GNR folds in a spiral manner, as in Figure 6e,f, without the necessity of heating. The formed helical structure is looser than in vacuum since the solvent molecules fill the gaps between the individual GNR stripes. Very recently, spontaneous formation of carbon nanoscrolls on CNTs has been also simulated on a substrate.[33]

CONCLUSIONS

In summary, we have demonstrated that carbon nanotubes can activate and guide the self-assembly of planar graphene nanostructures on their surfaces and in their interiors in vacuum and in solvents. Since the presented processes depend on the initial conditions, we can call them more precisely a controlled or guided self-assembly. The self-assembly can proceed by sliding, folding, and rolling motions, leading to stable or metastable bulky nanostructures, such as knots, rings, and helices. In the case of GNRs self-assembled on CNTs, the GNR−CNT coupling energy increases from the least stable helical locked phase to the helical phase and the stable straight phase. For GNRs and CNTs with different symmetries, other possible arrangements might be formed and stabilized differently. The GNRs can also hybridize with

other nanostructures. The novel hybrid materials are expected to have unique mechanical, electrical, and optical properties[34] and numerous potential applications.

METHODS

We model the self-assembly processes by atomistic molecular dynamics (MD) simulations with the NAMD package and the CHARMM27 force field.[35,36] The (nonbonding) vdW coupling between the *i*th and *j*th carbon atoms in the CNTs and graphene is described by the Lennard-Jones potential

$$V_{i,j} = \varepsilon_C \left[\left(\frac{r_{\min,C}}{r_{i,j}} \right)^{12} - 2 \left(\frac{r_{\min,C}}{r_{i,j}} \right)^{6} \right] \quad (4)$$

where $\varepsilon_C = -0.07$ kcal/mol and $r_{\min,C} = 3.98$ Å. The vdW coupling of other atoms is described in the CHARMM27 force field.[36] The systems are modeled in NVT ensembles at $T = 300$ K, and the time step is 1 fs. The Langevin damping[37] is used to thermalize the systems and mimic the missing electron coupling, while the phonon coupling is largely present in these simulations. We use a small damping coefficient of $\gamma = 0.01$ ps^{-1} that should be sufficient for this purpose.[23] The value of γ should be kept small since the Langevin dynamics does not preserve momentum during the self-assembly. In most cases, its value is not expected to significantly influence the observed folding dynamics, except of the folding speed. Electronic polarization of the studied systems is neglected. In all of the studied systems, GNRs have armchair structures along their long edges and CNTs have zigzag structures.

Acknowledgment. This work is supported by the NSF Grant CBET−0932812. The presented calculations have been partly realized on the NERSC supercomputer networks.

Supporting Information Available: Movies related to GNR rolling on a CNT surface, helix formation on the surface and inside the CNT, and knot formation on the CNT surface are prepared. This material is available free of charge *via* the Internet at http://pubs.acs.org.

REFERENCES AND NOTES

1. Novoselov, K. S.; Geim, A. K.; Morozov, S. V.; Jiang, D.; Zhang, Y.; Dubonos, S. V.; Grigorieva, I. V.; Firsov, A. A. Electric Field Effect in Atomically Thin Carbon Films. *Science* **2004,** *306*, 666–669.
2. Geim, A. K.; Novoselov, K. S. The Rise of Graphene. *Nat. Mater.* **2007,** *6*, 183–191.
3. Berner, S.; Corso, M.; Widmer, R.; Groening, O.; Laskowski, R.; Blaha, P.; Schwarz, K.; Goriachko, A.; Over, H.; Gsell, S.; *et al.* Boron Nitride Nanomesh: Functionality from a Corrugated Monolayer. *Angew. Chem., Int. Ed.* **2007,** *46*, 5115–5119.
4. Laskowski, R.; Blaha, P.; Gallauner, T.; Schwarz, K. Single-Layer Model of the Hexagonal Boron Nitride Nanomesh on the Rh(111) Surface. *Phys. Rev. Lett.* **2007,** *98*, 106802.
5. Li, X.; Wang, X.; Zhang, L.; Lee, S.; Dai, H. Chemically Derived, Ultrasmooth Graphene Nanoribbon Semiconductors. *Science* **2008,** *319*, 1229–1232.
6. Jiao, L.; Zhang, L.; Wang, X.; Diankov, G.; Dai, H. Narrow Graphene Nanoribbons from Carbon Nanotubes. *Nature* **2009,** *458*, 877–880.
7. Jiao, L.; Wang, X.; Diankov, G.; Wang, H.; Dai, H. Facile Synthesis of High-Quality Graphene Nanoribbons. *Nat. Nanotechnol.* **2010,** *5*, 321–325.
8. Kosynkin, D. V.; Higginbotham, A. L.; Sinitskii, A.; Lomeda, J. R.; Dimiev, A.; B. K. Price, B. K.; Tour, J. M. Longitudinal Unzipping of Carbon Canotubes To Form Graphene Nanoribbons. *Nature* **2009,** *458*, 872–876.
9. Tapasztó, L.; Dobrik, G.; Lambin, P.; Biró, L. P. Tailoring the Atomic Structure of Graphene Nanoribbons by Scanning Tunnelling Microscope Lithography. *Nat. Nanotechnol.* **2008,** *3*, 397–401.
10. Stampfer, C.; Guttinger, J.; Hellmuller, S.; Molitor, F.; Ensslin, K.; Ihn, T. Energy Gaps in Etched Graphene Nanoribbons. *Phys. Rev. Lett.* **2009,** *102*, 056403.
11. Ci, L.; Xu, Z.; Wang, L.; Gao, W.; Ding, F.; Kelly, K. F.; Yakobson, B. I.; Ajayan, P. M. Controlled Nanocutting of Graphene. *Nano Res.* **2008,** *1*, 116–122.
12. Campos, L. C.; Manfrinato, R. V.; Sanchez-Yamagishi, J. D.; Kong, J.; Jarillo-Herrero, P. Anisotropic Etching and Nanoribbon Formation in Single-Layer Graphene. *Nano Lett.* **2009,** *9*, 2600–2604.
13. Zhu, Z. P.; Su, D. S.; Weinberg, G.; Schlogl, R. Supermolecular Self-Assembly of Graphene Sheets: Formation of Tube-in-Tube Nanostructures. *Nano Lett.* **2004,** *4*, 2255–2259.
14. Jin, W.; Fukushima, T.; Niki, M.; Kosaka, A.; Ishii, N.; Aida, T. Self-Assembled Graphitic Nanotubes with One-Handed Helical Arrays of a Chiral Amphiphilic Molecular Graphene. *Proc. Natl. Acad. Sci. U.S.A.* **2005,** *102*, 10801–10806.
15. Chen, Q.; Chen, T.; Pan, G. B.; Yan, H. J.; Song, W. G.; Wan, L. J.; Li, Z. T.; Wang, Z. H.; Shang, B.; Yuan, L. F.; *et al.* Structural Selection of Graphene Supramolecular Assembly Oriented by Molecular Conformation and Alkyl Chain. *Proc. Natl. Acad. Sci. U.S.A.* **2008,** *105*, 16849–16854.
16. Lee, C.; Wei, X.; Kysar, J. W.; Hone, J. Measurement of the Elastic Properties and Intrinsic Strength of Monolayer Graphene. *Science* **2008,** *321*, 385–388.
17. Bunch, J. S.; Verbridge, S. S.; Alden, J. S.; van der Zande, A. M.; Parpia, J. M.; Craighead, H. G.; McEuen, P. L. Impermeable Atomic Membranes from Graphene Sheets. *Nano Lett.* **2008,** *8*, 2458–2462.
18. Gómez-Navarro, C.; Burghard, M.; Kern, K. Elastic Properties of Chemically Derived Single Graphene Sheets. *Nano Lett.* **2008,** *8*, 2045–2049.
19. Viculis, L. M.; Mack, J. J.; Kaner, R. B. A Chemical Route to Carbon Nanoscrolls. *Science* **2003,** *299*, 1361.
20. Braga, S. F.; Coluci, V. R.; Legoas, S. B.; Giro, R.; Galvao, D. S.; Baughman, R. H. Structure and Dynamics of Carbon Nanoscrolls. *Nano Lett.* **2004,** *4*, 881–884.
21. Yu, D.; Liu, F. Synthesis of Carbon Nanotubes by Rolling up Patterned Graphene Nanoribbons Using Selective Atomic Adsorption. *Nano Lett.* **2007,** *7*, 3046–3050.
22. Sidorov, A.; Mudd, D.; Sumanasekera, G; Ouseph, P. J.; Jayanthi, C. S.; Wu, S.-Y. Electrostatic Deposition of Graphene in a Gaseous Environment: A Deterministic Route for Synthesizing Rolled Graphenes? *Nanotechnology* **2009,** *20*, 055611.
23. Patra, N.; Wang, B.; Král, P. Nanodroplet Activated and Guided Folding of Graphene Nanostructures. *Nano Lett.* **2009,** *9*, 3766–3771.
24. Buldum, A.; Lu, J. P. Atomic Scale Sliding and Rolling of Carbon Nanotubes. *Phys. Rev. Lett.* **1999,** *83*, 5050–5053.
25. Ortolani, L.; Houdellier, F.; Monthioux, M.; Morandi, V. Chirality Dependent Surface Adhesion of Single-Walled Carbon Nanotubes on Graphene Surfaces. *Carbon* **2010,** *48*, 3050–3056.
26. Wang, B.; Král, P.; Thanopulos, I. Docking of Chiral Molecules on Twisted and Helical Nanotubes: Nanomechanical Control of Catalysis. *Nano Lett.* **2006,** *6*, 1918–1921.
27. Lu, Q.; Arroyo, M.; Huang, R. Elastic Bending Modulus of Monolayer Graphene. *J. Phys. D: Appl. Phys.* **2009,** *42*, 102002–102007.
28. Atalaya, J.; Isacsson, A.; Kinaret, J. M. Continuum Elastic Modeling of Graphene Resonators. *Nano Lett.* **2008,** *8*, 4196–4200.

29. (1) We evaluate σ_{sym} by placing a small ($\approx$9.1 nm^2) relaxed hexagonal piece of graphene on a large fixed square graphene. After relaxation, they adjust their positions to (graphite-like) AB-form interlayer stacking (half of the atoms sitting above each other). We assign the angle of $\varphi = 0$ to this locked orientation. Then, we rotate the hexagonal graphene flake around its center and calculate by VMD the total energy ($T = 20$ K). The E_{C-G} total energy has a C_6 symmetry: it increases sharply at the first $\Delta\varphi \approx 3°$ of rotation and keeps relatively constant until it sharply returns to its minimum energy at $\varphi = 60°$, and so on. The CNT−GNR binding energy density, $\langle\sigma_{C-G}\rangle$, is calculated as the maximum (in value) vdW energy per unit area of the system ($\varphi = 30°$). Due to sharp localization of the energy minima, we consider nonzero σ_{sym} only at $\varphi = n60°$ and define it as the energy difference per unit area between the energy maxima ($\varphi = 30°$) and minima points ($\varphi = 0$). Averaging of the energies is done over 100 consecutive frames of the simulation trajectory, with a 1 ps time interval. (2) The GNR−GNR sidewise vdW energy density, σ_{G-G}, is calculated as the difference of the (averaged) energies per unit length of two GNRs placed in a plane and separated by 0.35 and 5 nm (both fixed). Their armchair structures are facing each other without any sidewise shifting. (3) In order to validate the CHARMM27 force field parameters, we calculate the flexural rigidity, as in ref 23, the Young's modulus of graphene (GNR), as in ref 30, and the average graphene−graphene vdW binding energy. We obtain the flexural rigidity of $D \approx 27.9$ kcal/mol and the Young's modulus of $E \approx 0.9$ TPa, where the used bond and angular constants are 322.5 kcal mol^{-1} Å^{-2} and 53.35 kcal mol^{-1} rad^{-2}, respectively. The average graphene−graphene vdW energy is 56 kcal/mol/nm^2 (0.024 eV/Å^2).
30. Titov, A.; Král, P.; Pearson, R. Sandwiched Graphene-Membrane Superstructures. *ACS Nano* **2010,** *4*, 229–234.
31. Humphrey, W.; Dalke, A.; Schulten, K. VMD: Visual Molecular Dynamics. *J. Mol. Graphics* **1996,** *14*, 33–38.
32. Wang, B.; Král, P. Optimal Atomistic Modifications of Material Surfaces: Design of Selective Nesting Sites for Biomolecules. *Small* **2007,** *3*, 580–584.
33. Zhang, Z.; Li, T. Carbon Nanotube Initiated Formation of Carbon Nanoscrolls. *Appl. Phys. Lett.* **2010,** *97*, 081909-3.
34. Baughman, R. H.; Cui, C. X.; Zakhidov, A. A.; Iqbal, Z.; Barisci, J. N.; Spinks, G. M.; Wallace, G. G.; Mazzoldi, A.; De Rossi, D.; Rinzler, A. G.; *et al.* Carbon Nanotube Actuators. *Science* **1999,** *284*, 1340–1344.
35. Phillips, J. C.; Braun, R.; Wang, W.; Gumbart, J.; Tajkhorshid, E.; Villa, E.; Chipot, C.; Skeel, R. D.; Kale, L.; Schulten, K. J. Scalable Molecular Dynamics with NAMD. *Comput. Chem.* **2005,** *26*, 1781–1802.
36. MacKerell, A. D., Jr.; Bashford, D.; Bellott, M.; Dunbrack, R. L., Jr.; Evanseck, J. D.; Field, M. J.; Fischer, S.; Gao, J.; Guo, H.; Ha, S.; *et al.* All-Atom Empirical Potential for Molecular Modeling and Dynamics Studies of Proteins. *J. Phys. Chem. B* **1998,** *102*, 3586–3617.
37. Servantie, J.; Gaspard, P. Methods of Calculation of a Friction Coefficient: Application to Nanotubes. *Phys. Rev. Lett.* **2003,** *91*, 185503.